

Approximate propagation of normal distributions for stochastic optimal control of nonsmooth systems*

Florian Messerer^a, Katrin Baumgärtner^a, Armin Nurkanović^a, Moritz Diehl^{a,b}

^a*Department of Microsystems Engineering (IMTEK), University of Freiburg, Georges-Koehler-Allee 102, 79110 Freiburg, Germany*

^b*Department of Mathematics, University of Freiburg, 79104 Freiburg Germany*

Abstract

We present a method for the approximate propagation of mean and covariance of a probability distribution through ordinary differential equations (ODE) with discontinuous right-hand side. For piecewise affine systems, a normalization of the propagated probability distribution at every time step allows us to analytically compute the expectation integrals of the mean and covariance dynamics while explicitly taking into account the discontinuity. This leads to a natural smoothing of the discontinuity such that for relevant levels of uncertainty the resulting ODE can be integrated directly with standard schemes and it is neither necessary to prespecify the switching sequence nor to use a switch detection method. We then show how this result can be employed in the more general case of piecewise smooth functions based on a structure preserving linearization scheme. The resulting dynamics can be straightforwardly used within standard formulations of stochastic optimal control problems with chance constraints.

Keywords: Nonsmooth dynamics, stochastic optimal control, numerical optimal control, uncertain initial value

1. Introduction

In this paper we consider initial value problems (IVP) with uncertain initial value $x_0 \in \mathbb{R}^n$ which are defined by an ordinary differential equation (ODE) with discontinuous right-hand side. More specifically, we consider IVP of the form

$$x(0) = x_0, \quad x_0 \sim \mathcal{X}_0, \quad \dot{x} = f(x) \quad \text{with} \quad f(x) := \begin{cases} f_1(x), & \psi(x) < 0, \\ f_2(x), & \psi(x) > 0, \end{cases} \quad (1)$$

for $t \in [0, T] =: \mathbb{T}$ and with the initial uncertainty described by probability distribution \mathcal{X}_0 . The right-hand side is defined by the smooth modes f_1 , f_2 and the switching function ψ , such that depending on the sign of $\psi(x)$ the dynamics evolve according to f_1 or f_2 . The zero-level set of ψ defines the switching surface as $\mathbb{S}_\psi = \{x \in \mathbb{R}^n \mid \psi(x) = 0\}$, and for regularity we assume $\nabla \psi(x) \neq 0$ for all $x \in \mathbb{S}_\psi$. For rigorously treating the discontinuity, i.e., the case where $\psi(x) = 0$, we refer to the notion of Filippov differential inclusions [1]. We only consider the nondegenerate cases where

*This research was supported by DFG via project 424107692 on Robust MPC and by the EU via ELO-X 953348.

the solution to (1) is well defined. The main results will be derived for the case that f_1 , f_2 and ψ are affine, with an extension on how these results can be employed in the nonlinear case. Since our primary interest here is the simulation of the dynamics we consider an uncontrolled system. However, the results straightforwardly extend to the case where f additionally depends on a control input.

Nonsmooth dynamics arise in the modeling of a wide range of systems, especially in mechanics and robotics, e.g., Coulomb friction, contact models, gear boxes, but also in electrical circuits [2, 3]. Since standard theory of numerical integration of ODE is built on the assumption of Lipschitz continuity [4] special care needs to be taken when simulating nonsmooth dynamics, for which this assumption is violated [2]. Based on a dynamic system model, optimal control provides a systematic framework for achieving a desired system behavior, i.e., optimizing trajectories based on an objective function and subject to constraints. Its closed loop application, model predictive control (MPC), relies on the numerical solution of optimal control problems (OCP) in real time [5]. Often this takes the form of solving nonlinear programs (NLP) via Newton-type, i.e., derivative based, methods [6]. Thus, when simulating system dynamics in this context, it is relevant that the integration schemes are both efficient and provide accurate sensitivities.

Since models typically do not allow for a perfect prediction of reality, there is always some uncertainty involved. The closely related fields of robust and stochastic optimal control try to explicitly account for this mismatch [5, 7, 8, 9]. In the robust paradigm this takes the form of set based uncertainty models, whereas the stochastic approach is concerned with probability distributions. Numerically the resulting formulations can be very similar: for example, a positive definite matrix can both describe the shape of an ellipsoidal set and the covariance of a normal distribution (giving rise to ellipsoidal confidence sets), cf., e.g. [10, 11]. Thus, while working in a stochastic framework – the results in this paper exploit the smoothly decaying unbounded support of normal distributions – we will still draw from results in the robust optimization literature.

1.1. Contribution and outline

In this paper we present a method for the approximate propagation of mean and covariance of a probability distribution through an ODE in the form of (1). The method is based on (a) linearizing the right-hand side function at the current mean in terms of its components f_1 , f_2 , ψ , such that a piecewise affine function is obtained which preserves the discontinuous structure of f , (b) approximating the current probability distribution by a normal distribution which for piecewise affine f allows us to analytically compute the current change of mean and covariance. However, since this neglects the change of the higher-order moments, this does not lead to an exact propagation. Finally, we demonstrate how the derived dynamics can be used in a stochastic optimal control problem formulation with chance constraints.

We start by discussing the relevant background on ODE with discontinuous right-hand side in Section 2 and on IVP with uncertain initial value in Section 3. In Section 4 we provide a detailed discussion of the simplified setting of a scalar piecewise constant system to further the intuitive understanding. This is followed by the derivation of the main result for piecewise affine systems in Section 5, the extension to the piecewise smooth case in Section 6, and its application to stochastic OCP in Section 7, with a concluding Section 8.

1.2. Notation

For a multivariate function $f: \mathbb{R}^n \rightarrow \mathbb{R}^m$, $x \mapsto f(x)$, the gradient is defined as the transpose of the Jacobian, $\nabla f(x) = \frac{\partial f(x)}{\partial x}^\top$, such that $\nabla f(x) \in \mathbb{R}^{n \times m}$. For two vectors $x \in \mathbb{R}^n$, $y \in \mathbb{R}^m$ their

vertical concatenation is denoted by $(x, y) := [x^\top, y^\top]^\top$. The convex hull of two vectors $x, y \in \mathbb{R}^n$ is $\text{conv}(x, y) := \{(1 - \theta)x + \theta y \mid \theta \in [0, 1]\}$. If a symmetric matrix $S = A + A^\top$ is a sum of a matrix $A \in \mathbb{R}^{n \times n}$ and its transpose, we abbreviate this as $S = A + (\star)$.

2. Ordinary differential equations with discontinuous right-hand side

In this section we briefly summarize the relevant background on ODE with discontinuous right-hand side of the form (1), to the extent relevant in the context of numerical optimal control. For a more indepth discussion we refer especially to [12].

2.1. Nondegenerate switching cases

We distinguish between two nondegenerate switching cases [12], in which the solution trajectory is well defined:

1. Crossing the discontinuity: $\psi(x) = 0$ and both $\nabla\psi(x)^\top f_1(x) > 0$ and $\nabla\psi(x)^\top f_2(x) > 0$. In consequence $\frac{d\psi(x(t))}{dt} > 0$ immediately before and after the switching time such that the state immediately leaves the switching surface after reaching it, and crosses from $\psi(x) < 0$ to $\psi(x) > 0$. The case where the surface is crossed in the opposite direction is analogous.
2. Sliding mode (or trapped case): $\psi(x) = 0$ and $\nabla\psi(x)^\top f_1(x) > 0$ but $\nabla\psi(x)^\top f_2(x) < 0$. In this case, the solution will remain on the surface, i.e., $\frac{d\psi(x(t))}{dt} = 0$ after the switching time.

2.2. Numerical integration

Because f is discontinuous, the standard theory of ODE and their numerical integration does not hold since it is built on the assumption of (Lipschitz)-continuity of f [4]. Thus, when relying on standard integration schemes and their theory, the switch needs to be considered explicitly. Otherwise the standard results on the order of integration accuracy will not hold – in general for a stepsize h the error will be $\mathcal{O}(h)$ irrespective of the order of the scheme [2] – and the error in the sensitivities will even be independent of the step size [12, 13]. In the context of optimal control this requires either a predefined switching sequence or a switch detecting integration scheme which supplies correct sensitivities [2, 14, 15]. An intuitive and common workaround is to smoothen the right-hand side (1). This results in the smooth approximate dynamics

$$f_\sigma(x) = (1 - \alpha_\sigma(\psi(x)))f_1(x) + \alpha_\sigma(\psi(x))f_2(x), \quad (2)$$

where $\alpha_\sigma: \mathbb{R} \rightarrow \mathbb{R}$ is a smooth approximation of the Heaviside step function, parametrized by $\sigma > 0$ and with increasing accuracy as $\sigma \rightarrow 0$. One standard choice is $\alpha_\sigma(\xi) = (1 + \tanh(\xi/\sigma))/2$. However, the resulting ODE will be increasingly nonlinear and stiff for decreasing σ and require decreasingly small step sizes for sufficiently precise integration. Furthermore it can be shown that the integrator has to have a step size of $h = o(\sigma)$ in order for its sensitivities to be adequate [12, 13], which is an important requirement if it is to be used as a component in the formulation of a nonlinear program (NLP). Thus, one is in general well advised to carefully choose an appropriate integration scheme when handling an ODE with discontinuous right-hand side.

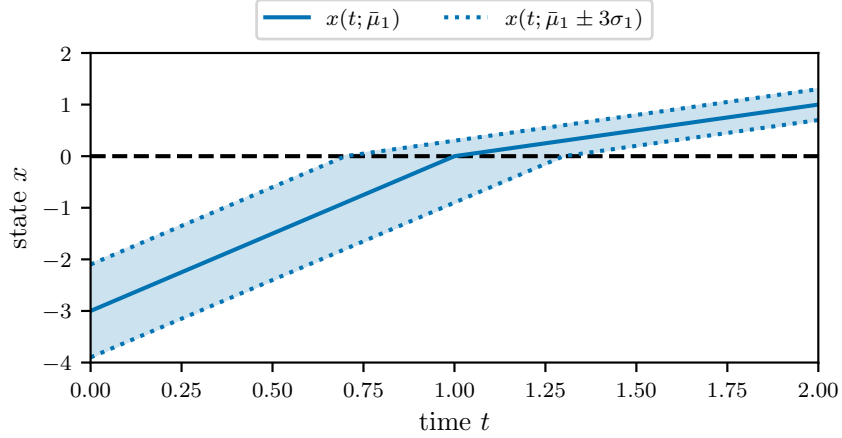


Figure 1: The state trajectories from Example 1. The switch at $x = 0$ leads to a kink in each trajectory and to a scaling of their distances with respect to each other.

2.3. Solution sensitivities

While the solution maps of IVP with discontinuous right-hand side are continuous, their sensitivities may have jumps when encountering a switch. Denote by $x(t; x_0)$, $t \in \mathbb{T}$, the solution of IVP (1) for a given initial value x_0 . Assume the IVP is not initialized at a switch but that at some time $0 < t_s < T$ with $x_s := x(t_s; x_0)$ the solution reaches the switching surface, $\psi(x_s) = 0$ and $\psi(x(t, x_0)) \neq 0$ for all $t \in [0, t_s]$. Then the sensitivity of the final state with respect to the initial value is given by

$$\frac{\partial x(T; x_0)}{\partial x_0} = \frac{\partial x(T - t_s; x_s)}{\partial x_s} J(x_s) \frac{\partial x(t_s; x_0)}{\partial x_0}, \quad (3)$$

where the jump matrix $J(x_s)$ accounts for the jump of sensitivity and is given by

$$J(x_s) = I + \frac{(f_2(x_s) - f_1(x_s)) \nabla \psi(x_s)^\top}{\nabla \psi(x_s)^\top f_1(x_s)} \quad \text{resp.} \quad J(x_s) = I + \frac{(f_2(x_s) - f_1(x_s)) \nabla \psi(x_s)^\top}{\nabla \psi(x_s)^\top ((f_1(x_s) - f_2(x_s)))} \quad (4)$$

for the crossing resp. sliding mode [12]. Without loss of generality, the jump matrix for the crossing case is given under the assumption that $\psi(x_0) < 0$, i.e., the state crosses from mode f_1 into mode f_2 .

Example 1 (Crossing the discontinuity). Consider a scalar system with state $x \in \mathbb{R}$ and $\dot{x} = 3$ for $x < 0$ and $\dot{x} = 1$ for $x > 0$. We simulate the trajectory $x(t; x_0)$ for three different values of the initial state x_0 , given by the set $\{\bar{\mu}_1, \bar{\mu}_1 + 3\sigma_1, \bar{\mu}_1 - 3\sigma_1\}$, with $\bar{\mu}_1 = -3$ and $\sigma_1 = 0.3$. The resulting trajectories are shown in Fig. 1. We observe that the discontinuity in \dot{x} at $x = 0$ leads to a kink in the trajectories. Due to this kink, the distance between the trajectories narrows. Whereas initially the distance between the two outer points is $6\sigma_1$, after each point has crossed the switch this distance has narrowed to $\frac{\bar{f}_2}{\bar{f}_1} 6\sigma_1 = \frac{1}{3} 6\sigma_1$. The scaling factor of $\frac{1}{3}$ is the same as the value of the corresponding jump matrix (4).

3. Initial value problems with uncertain initial value

We now consider again a general IVP with $x(0) = x_0$, $\dot{x} = f(x)$, $t \in \mathbb{T}$, and assume its solution is well defined for every $x_0 \in \mathbb{R}^n$. However, the initial state is not exactly known. Instead it follows

a probability distribution, $x_0 \sim \mathcal{X}_0$. If we denote by $x(t; x_0)$ the solution to the IVP after the time interval $[0, t]$ given $x(0) = x_0$, this induces a distribution $\mathcal{X}(t)$ over the solution trajectory such that $x(t; x_0) \sim \mathcal{X}(t)$. Alternatively we can view this as an IVP in distribution space, $\mathcal{X}(0) = \mathcal{X}_0$, $\dot{\mathcal{X}} = \mathcal{F}(\mathcal{X})$, with appropriately defined \mathcal{F} .

In principle, we can describe this evolution in terms of the moments of \mathcal{X} , assuming that all moments are finite and uniquely determine \mathcal{X} . This holds if \mathcal{X} has bounded support or if its tails decay sufficiently fast, which includes normal distributions [16]. In particular, consider the first and second-order moments, mean and covariance, defined as

$$\mathbf{m}_{\mathcal{X}} := \mathbb{E}_{x \sim \mathcal{X}}\{x\} \quad (5a)$$

$$\text{cov}_{\mathcal{X}} := \mathbb{E}_{x \sim \mathcal{X}}\{(x - \mathbf{m}_{\mathcal{X}})(x - \mathbf{m}_{\mathcal{X}})^\top\} \quad (5b)$$

Noting that $\mathbb{E}_{x \sim \mathcal{X}(t)}\{x\} = \mathbb{E}_{x_0 \sim \mathcal{X}_0}\{x(t; x_0)\}$, we get the time derivative of the mean as

$$\frac{d}{dt} \mathbf{m}_{\mathcal{X}(t)} = \frac{d}{dt} \mathbb{E}_{x_0 \sim \mathcal{X}_0}\{x(t; x_0)\} = \mathbb{E}_{x_0 \sim \mathcal{X}_0}\{\frac{d}{dt}x(t; x_0)\} = \mathbb{E}_{x \sim \mathcal{X}(t)}\{f(x)\}. \quad (6a)$$

Similarly, we get the time derivative of the covariance as

$$\frac{d}{dt} \text{cov}_{\mathcal{X}} = \frac{d}{dt} \mathbb{E}_{x \sim \mathcal{X}}\{(x - \mathbf{m}_{\mathcal{X}})(x - \mathbf{m}_{\mathcal{X}})^\top\} \quad (6b)$$

$$= \mathbb{E}_{x \sim \mathcal{X}}\{(f(x) - \frac{d}{dt} \mathbf{m}_{\mathcal{X}})(x - \mathbf{m}_{\mathcal{X}})^\top + (\star)\} \quad (6c)$$

$$= \mathbb{E}_{x \sim \mathcal{X}}\{f(x)(x - \mathbf{m}_{\mathcal{X}})^\top\} + (\star). \quad (6d)$$

However, to exactly describe the evolution of \mathcal{X} , we would need to consider the change of all moments up to infinite order, which is in general intractable. Further, we cannot treat the expectation of a nonlinear transformation of a random variable in this general setting.

3.1. Linearization-based uncertainty propagation for smooth dynamics

For IVP with smooth dynamics (or in general for smooth nonlinear transformations of random variables) a standard approach to approximate the uncertainty propagation is based on linearization. Examples include widely used methods such as the Extended Kalman Filter [17]. There are two major variants: (i) linearization of the right-hand side of the ODE, and (ii) linearization of the integration map.

In the first variant, after substituting f by its first-order Taylor approximation at the mean, the expectations in (6) can be analytically computed as

$$\frac{d}{dt} \mathbf{m}_{\mathcal{X}} \approx \mathbb{E}_{x \sim \mathcal{X}}\{f(\mathbf{m}_{\mathcal{X}}) + \frac{\partial f(\mathbf{m}_{\mathcal{X}})}{\partial \mathbf{m}_{\mathcal{X}}}(x - \mathbf{m}_{\mathcal{X}})\} = f(\mathbf{m}_{\mathcal{X}}), \quad (7a)$$

$$\frac{d}{dt} \text{cov}_{\mathcal{X}} \approx \mathbb{E}_{x \sim \mathcal{X}}\{(f(\mathbf{m}_{\mathcal{X}}) + \frac{\partial f(\mathbf{m}_{\mathcal{X}})}{\partial \mathbf{m}_{\mathcal{X}}}(x - \mathbf{m}_{\mathcal{X}}))(x - \mathbf{m}_{\mathcal{X}})^\top\} + (\star) = \frac{\partial f(\mathbf{m}_{\mathcal{X}})}{\partial \mathbf{m}_{\mathcal{X}}} \text{cov}_{\mathcal{X}} + (\star). \quad (7b)$$

This is exact for the case that f is an affine function. Thus, the resulting approximate propagation of the first two moments is defined by the IVP

$$\mu(0) = \mathbf{m}_{\mathcal{X}_0}, \quad \dot{\mu} = f(\mu), \quad (8a)$$

$$\Sigma(0) = \text{cov}_{\mathcal{X}_0}, \quad \dot{\Sigma} = \frac{\partial f(\mu)}{\partial \mu} \Sigma + \Sigma \frac{\partial f(\mu)}{\partial \mu}^\top. \quad (8b)$$

Unsurprisingly, the covariance dynamics are in the form of the continuous time differential Lyapunov equation [18], i.e., the covariance dynamics of a linear system.

While in the preceding approach the uncertainty propagation is given in continuous time, in direct optimal control the dynamics are usually considered only on a discrete time grid. Thus an alternative approach, corresponding to the second variant, is to discretize the dynamics first and only then consider uncertainty. Let $f_h(x_k) := x(h; x_k)$ denote the integration of the dynamics over the discretization time step h given the initial value x_k , such that $x_{k+1} = f_h(x_k)$. Then, given $x_k \sim \mathcal{X}_k$, we can approximate the expectations as

$$m_{\mathcal{X}_{k+1}} = \mathbb{E}_{x \sim \mathcal{X}_k} \{f_h(x)\} \quad (9a)$$

$$\approx \mathbb{E}_{x \sim \mathcal{X}_k} \{f_h(m_{\mathcal{X}_k}) + \frac{\partial f_h(m_{\mathcal{X}_k})}{\partial m_{\mathcal{X}_k}}(x - m_{\mathcal{X}_k})\} = f_h(m_{\mathcal{X}_k}), \quad (9b)$$

$$\text{cov}_{\mathcal{X}_{k+1}} = \mathbb{E}_{x \sim \mathcal{X}_k} \{(f_h(x) - m_{\mathcal{X}_{k+1}})(f_h(x) - m_{\mathcal{X}_{k+1}})^\top\} \quad (9c)$$

$$\approx \mathbb{E}_{x \sim \mathcal{X}_k} \left\{ \frac{\partial f_h(m_{\mathcal{X}_k})}{\partial m_{\mathcal{X}_k}}(x - m_{\mathcal{X}_k})(x - m_{\mathcal{X}_k})^\top \frac{\partial f_h(m_{\mathcal{X}_k})}{\partial m_{\mathcal{X}_k}}^\top \right\} = \frac{\partial f_h(m_{\mathcal{X}_k})}{\partial m_{\mathcal{X}_k}} \text{cov}_{\mathcal{X}_k} \frac{\partial f_h(m_{\mathcal{X}_k})}{\partial m_{\mathcal{X}_k}}^\top. \quad (9d)$$

This results in the approximate propagation

$$\mu_0 = m_{\mathcal{X}_0}, \quad \mu_{k+1} = f_h(\mu_k), \quad (10a)$$

$$\Sigma_0 = \text{cov}_{\mathcal{X}_0}, \quad \Sigma_{k+1} = \frac{\partial f_h(\mu_k)}{\partial \mu_k} \Sigma_k \frac{\partial f_h(\mu_k)}{\partial \mu_k}^\top, \quad (10b)$$

with the covariance dynamic corresponding to the discrete time Lyapunov difference equation. While during the numerical integration of (8) it can happen that Σ takes indefinite values, the propagation in (10) guarantees that $\Sigma_k \succeq 0$ if $\Sigma_0 \succeq 0$, cf. [19].

3.2. Linearization-based uncertainty propagation for nonsmooth dynamics

Both of the approaches discussed in the previous subsection rely on linearization of a smooth function. Thus, they are not directly applicable to ODE with a discontinuous right-hand side. Again, an intuitive approach is to smoothen the dynamics as in (2) and then apply a linearization based scheme. This does not come without issues: all the problems regarding stiffness and accuracy of derivatives from the nominal case will transfer such that it is challenging to use within an optimization problem, cf. Section 2.2. Thus, as in the nominal case, an alternative is to treat the switch explicitly and propagate the covariance based on (10). Using the jump matrix (4) the sensitivity jump can be handled explicitly. However, in the context of optimal control this requires either a method for switch detection [20] or a predefined switching sequence.

Furthermore, the linearization based propagation of mean and covariance leans on the assumption that the nonlinear dynamics are sufficiently well approximated by a linearization at the mean within the region of uncertainty. For a switched system this is clearly not the case if the mean is on one side of the switch but a nonnegligible amount of probability mass on the other. While this works for some situations, in others it can cause a complete failure of the uncertainty propagation as we will see in a later example.

3.3. Normalization-based uncertainty propagation

In the remainder of this paper we will derive an alternative method for the approximate propagation of mean and covariance. Instead of linearization the method is based on “normalization” of the probability distribution, i.e., at each point in time we approximate the true distribution by a normal distribution that is defined by our current value for mean and variance. For switched affine systems this will allow us to compute the expectations in (6) analytically, resulting in a natural smoothing of the discontinuity. This yields an easy to implement ODE for mean and variance that can be treated by standard integrators and be straightforwardly used within tractable stochastic OCP formulations.

A similar idea of renormalization after every time step (although in a discrete time setting) is used in the method of moment matching for recursive time series prediction based on Gaussian process models: for these, the mean and covariance of the output can be exactly computed given a normal distribution in the input variable [21]. Further, unscented Kalman filter [22] discretizes the current normal distribution into systematically chosen samples which are then propagated through the nonlinear function. Based on mean and variance of the propagated samples, a new normal distribution is obtained.

While we will explain our suggested approach in detail in the following three sections, we already derive some results that will be useful later on. Assume that at our current time point the state follows a n -variate normal distribution, $x \sim \mathcal{N}(\mu, \Sigma)$, with probability density function (PDF) given by

$$\tilde{\phi}(x; \mu, \Sigma) = \frac{1}{\sqrt{(2\pi)^n \det \Sigma}} e^{-\frac{1}{2}(x-\mu)^\top \Sigma^{-1}(x-\mu)}. \quad (11)$$

We propagate the first two moments for an infinitesimal time step based on this assumption. In this case the following lemma holds.

Lemma 2. *Consider the IVP $x(0) = x_0$, $\dot{x} = f(x)$, $t \in \mathbb{T}$, with uncertain initial value $x_0 \sim \mathcal{X}_0$. This defines a distribution in state space $\mathcal{X}(t)$ for every $t \in \mathbb{T}$. Assume that at some time $\bar{t} \in \mathbb{T}$ the state is normally distributed, $x(\bar{t}) \sim \mathcal{X}(\bar{t}) = \mathcal{N}(\mu, \Sigma)$, such that $\mathbf{m}_{\mathcal{X}(\bar{t})} = \mu$ and $\mathbf{cov}_{\mathcal{X}(\bar{t})} = \Sigma$. Then, at this exact time, mean and variance evolve as*

$$\frac{d}{dt} \mathbf{m}_{\mathcal{X}} = \mathbb{E}_{x \sim \mathcal{N}(\mu, \Sigma)} \{f(x)\} =: \hat{f}_\mu(\mu, \Sigma), \quad (12a)$$

$$\frac{d}{dt} \mathbf{cov}_{\mathcal{X}} = \frac{\partial \hat{f}_\mu(\mu, \Sigma)}{\partial \mu} \Sigma + \Sigma \frac{\partial \hat{f}_\mu(\mu, \Sigma)}{\partial \mu}^\top =: \hat{f}_\Sigma(\mu, \Sigma). \quad (12b)$$

Remark 3. In general the distribution \mathcal{X} will not stay a normal distribution since the higher-order moments evolve differently. Thus the assumption $\mathcal{X} = \mathcal{N}(\mu, \Sigma)$ will not hold anymore after the first infinitesimal time step.

Proof. The mean dynamics $\frac{d}{dt} m_{\mathcal{X}}$ we have directly from (6a). For $\frac{d}{dt} \text{cov}_{\mathcal{X}}$ we rearrange (6d) as

$$\frac{d}{dt} \text{cov}_{\mathcal{X}} = \mathbb{E}_{x \sim \mathcal{X}} \{f(x)(x - m_{\mathcal{X}})^\top\} + (\star) \quad (13a)$$

$$= \mathbb{E}_{x \sim \mathcal{N}(\mu, \Sigma)} \{f(x)(x - \mu)^\top\} + (\star) \quad (13b)$$

$$= \int_{\mathbb{R}^n} f(x)(x - \mu)^\top \tilde{\phi}(x; \mu, \Sigma) dx + (\star) \quad (13c)$$

$$= \int_{\mathbb{R}^n} f(x)(x - \mu)^\top \tilde{\phi}(x; \mu, \Sigma) \Sigma^{-1} \Sigma dx + (\star) \quad (13d)$$

$$= \left(\int_{\mathbb{R}^n} f(x) \tilde{\phi}(x; \mu, \Sigma) (x - \mu)^\top \Sigma^{-1} dx \right) \Sigma + (\star) \quad (13e)$$

$$= \left(\int_{\mathbb{R}^n} f(x) \left(\frac{\partial}{\partial \mu} \tilde{\phi}(x; \mu, \Sigma) \right) dx \right) \Sigma + (\star) \quad (13f)$$

$$= \left(\frac{\partial}{\partial \mu} \int_{\mathbb{R}^n} f(x) \tilde{\phi}(x; \mu, \Sigma) dx \right) \Sigma + (\star) \quad (13g)$$

$$= \left(\frac{\partial}{\partial \mu} \mathbb{E}_{x \sim \mathcal{N}(\mu, \Sigma)} \{f(x)\} \right) \Sigma + (\star) \quad (13h)$$

$$= \frac{\partial \hat{f}_\mu(\mu, \Sigma)}{\partial \mu} \Sigma + (\star) \quad (13i)$$

where in (13e) we used $\frac{\partial}{\partial \mu} \tilde{\phi}(x; \mu, \Sigma) = \tilde{\phi}(x; \mu, \Sigma)(x - \mu)^\top \Sigma^{-1}$. \square

Once we have accepted that we cannot propagate the distribution exactly, this lemma comes in very useful: If we can find a closed-form expression for the mean dynamics $\dot{\mu}$, we get a closed-form expression of the variance dynamics $\dot{\Sigma}$ for free. Our main idea is now to propagate μ and Σ according to these dynamics, and approximate the state distribution at each time by $\mathcal{N}(\mu, \Sigma)$.

Definition 4. Consider the IVP $x(0) = x_0$, $\dot{x} = f(x)$, $t \in \mathbb{T}$, $x_0 \sim \mathcal{N}(\mu, \Sigma) = \mathcal{X}_0$. Assume $x(t; x_0)$ is well defined for all $x_0 \in \mathbb{R}$, $t \in \mathbb{T}$, and that all moments of \mathcal{X}_0 are finite and uniquely determine \mathcal{X}_0 . This defines a time-dependent state distribution \mathcal{X} via $\mathcal{X}(0) = \mathcal{X}_0$, $\dot{\mathcal{X}} = \mathcal{F}(\mathcal{X})$. Further consider the IVP

$$\mu(0) = \mu_0, \quad \dot{\mu} = \hat{f}_\mu(\mu, \Sigma), \quad (14a)$$

$$\Sigma(0) = \Sigma_0, \quad \dot{\Sigma} = \hat{f}_\Sigma(\mu, \Sigma), \quad (14b)$$

inducing for each t the state distribution $\mathcal{N}(\mu, \Sigma)$. Then, for each t this defines an error by the difference of the distributions $\mathcal{X}(t)$ and $\mathcal{N}(\mu(t), \Sigma(t))$. More specifically, we can characterize it by the difference of the moments of these distributions. In particular, we consider the error in the mean, $\tilde{\mu} = m(\tilde{\mathcal{X}}) = m_{\mathcal{X}} - \mu$ and the covariance, $\tilde{\Sigma} = \text{cov}_{\mathcal{X}} - \Sigma$.

We conclude this section with a small lemma which we will use several times throughout the paper. Before stating the lemma and with a slight overload of notation, we define the probability density function of the standard normal distribution as

$$\phi(\nu) := \tilde{\phi}(\nu; 0, 1) = \frac{1}{\sqrt{2\pi}} e^{-\frac{1}{2}\nu^2}, \quad \Phi(\nu) = \int_{-\infty}^{\nu} \phi(\nu') d\nu', \quad (15)$$

with associated cumulative distribution function (CDF) Φ . While there exists no closed-form expression for Φ , we can in practice treat it as such since numerical implementations are readily available via the error function $\text{erf}(\cdot)$.

Lemma 5. *Let $\alpha, \beta, \xi, \bar{\xi}, \mu, \sigma \in \mathbb{R}$, $\sigma > 0$. Then*

$$\int_{-\infty}^{\bar{\xi}} (\alpha\xi + \beta)\tilde{\phi}(\xi; \mu, \sigma^2) d\xi = -\alpha\sigma^2 \frac{1}{\sigma} \phi\left(\frac{\bar{\xi}-\mu}{\sigma}\right) + (\alpha\mu + \beta)\Phi\left(\frac{\bar{\xi}-\mu}{\sigma}\right) \quad (16a)$$

$$\int_{\bar{\xi}}^{\infty} (\alpha\xi + \beta)\tilde{\phi}(\xi; \mu, \sigma^2) d\xi = \alpha\sigma^2 \frac{1}{\sigma} \phi\left(\frac{\bar{\xi}-\mu}{\sigma}\right) + (\alpha\mu + \beta)(1 - \Phi\left(\frac{\bar{\xi}-\mu}{\sigma}\right)) \quad (16b)$$

Proof. For (16a) we have

$$\int_{-\infty}^{\bar{\xi}} (\alpha\xi + \beta)\tilde{\phi}(\xi; \mu, \sigma^2) d\xi = \int_{-\infty}^{\frac{\bar{\xi}-\mu}{\sigma}} (\alpha(\sigma\nu + \mu) + \beta)\phi(\nu) d\nu \quad (17a)$$

$$= \alpha\sigma \int_{-\infty}^{\frac{\bar{\xi}-\mu}{\sigma}} \nu\phi(\nu) d\nu + (\alpha\mu + \beta) \int_{-\infty}^{\frac{\bar{\xi}-\mu}{\sigma}} \phi(\nu) d\nu \quad (17b)$$

$$= -\alpha\sigma^2 \frac{1}{\sigma} \phi\left(\frac{\bar{\xi}-\mu}{\sigma}\right) + (\alpha\mu + \beta)\Phi\left(\frac{\bar{\xi}-\mu}{\sigma}\right), \quad (17c)$$

where in the first line we substituted $\xi = \sigma\nu + \mu$. For (16b) the derivation is similar.

4. Uncertainty propagation for scalar piecewise constant systems

In order to get an intuitive understanding of how a normal distribution behaves when encountering a discontinuity, we will first limit our analysis to a scalar state space $x \in \mathbb{R}$ with piecewise constant dynamics $\dot{x} = f(x)$ of the form

$$f(x) = \begin{cases} \bar{f}_1, & x < 0, \\ \bar{f}_2, & x > 0, \end{cases} \quad (18)$$

with $\bar{f}_1, \bar{f}_2 \in \mathbb{R} \setminus \{0\}$. If \bar{f}_1 and \bar{f}_2 have the same sign, this leads to a crossing of the discontinuity, whereas $\bar{f}_1 > 0$ and $\bar{f}_2 < 0$ leads to the sliding mode. In the following we will first take a detailed look at how a normal distribution behaves when crossing the discontinuity, which is then followed by an approximate approach for propagating its first two moments.

4.1. Case study: a switched normal distribution crossing the discontinuity

We start by revisiting Example 1.

Example 6 (Crossing the discontinuity (cont.)). Consider again the system from Example 1, i.e., dynamics in the form of (18) with $\bar{f}_1 = 3$ and $\bar{f}_2 = 1$. This time, assume that the initial value x_0 follows a normal distribution, $x_0 \in \mathcal{N}(\bar{\mu}_1, \sigma_1^2)$, with $\bar{\mu}_1 = -3$, $\sigma_1 = 0.3$. For ease of presentation, we first limit our attention to the interval $x_0 \in [\bar{\mu}_1 - 3\sigma_1, \bar{\mu}_1 + 3\sigma_1]$, noting that it contains around 99.7% of the probability mass. Consistent with the behavior we saw in the previous example, after each point of the interval has passed through the discontinuity, the distribution has been scaled by factor $\frac{\bar{f}_2}{\bar{f}_1} = \frac{1}{3}$, such that now the state is distributed as $\mathcal{N}(x(t; \bar{\mu}_1), \sigma_2)$ with $\sigma_2 = \frac{\bar{f}_2}{\bar{f}_1} \sigma_1 = \frac{1}{3} \sigma_1$, see Fig. 2 (left). This has to hold since the scaling applies to any two arbitrarily chosen points from the interval, as long as both points start on one side of the discontinuity and end on the other.

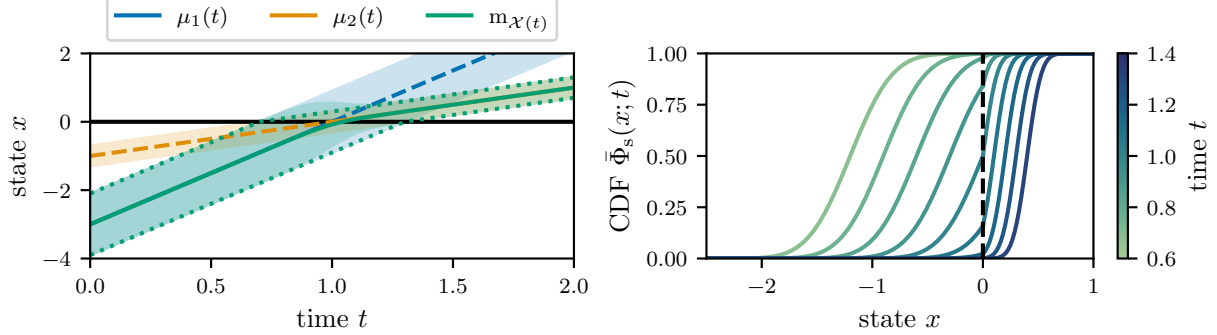


Figure 2: Left: The means of the two imagined normal distributions $\mathcal{N}(\mu_i(t), \sigma_i^2)$, $i = 1, 2$, compared to the mean of the exactly propagated distribution. The shaded regions indicate 3σ on each side of the mean. The dotted lines indicate the 99.7% probability mass corresponding to the original $\pm 3\sigma$ region. Right: The cumulative density function $\bar{\Phi}_s(x; \mu_1(t), \mu_2(t), \sigma_1, \sigma_2)$ of the switched normal distribution for various time points as the distribution crosses the switch at $x = 0$.

Since $\bar{\mu}_1$ is the median of the initial distribution, with 50% of probability mass on each side of $\bar{\mu}_1$, it follows that as the system evolves $x(t; \bar{\mu}_1)$ will always be the median of the evolved distribution. However, since the points above $x(t; \bar{\mu}_1)$ are squeezed together earlier than those below, the mean will be below the median while the distribution is crossing the discontinuity.

We observe that in the example there are two virtual normal distributions involved, visualized in Fig. 2 (left). The first one is associated with points below the switch and given by $\mathcal{N}(\mu_1(t), \sigma_1^2)$, with the evolution of its mean defined by $\mu_1(0) = \bar{\mu}_1$ and $\dot{\mu}_1 = \bar{f}_1$, such that $\mu_1(t) = \bar{\mu}_1 + \bar{f}_1 t$. The second distribution is $\mathcal{N}(\mu_2(t), \sigma_2^2)$ with $\dot{\mu}_2 = \bar{f}_2$. Further, there is a time point t_s such that $\mu_1(t_s) = \mu_2(t_s) = 0$. In the considered example, this is $t_s = 1$. From these conditions we can compute $\bar{\mu}_2 = \frac{\bar{f}_2}{\bar{f}_1} \bar{\mu}_1$ such that $\mu_2(t) = \bar{\mu}_2 + \bar{f}_2 t$.

We now revisit the assumption that $x_0 \in \mathcal{N}(\bar{\mu}_1, \sigma_1^2)$. While this is certainly a valid assumption, it is slightly inconsistent: It makes a statement about all points, including those above the switching surface. But we have seen that as soon as an interval of points passes the discontinuity, their distribution is scaled such that it will be closely related to $\mathcal{N}(\mu_2(t), \sigma_2^2)$. With this in mind, it seems more natural to assume that the distribution for all points above the switch has already been transformed. In consequence, we can describe the distribution at time t as

$$x(t) \sim \mathcal{N}_s(\mu_1(t), \mu_2(t), \sigma_1^2, \sigma_2^2), \quad (19)$$

where $\mu_1(t)$, $\mu_2(t)$, σ_1 , σ_2 are as defined above, and which is defined via its PDF

$$\bar{\phi}_s(x; \mu_1, \mu_2, \sigma_1, \sigma_2) = \begin{cases} \frac{1}{\sigma_1} \phi\left(\frac{x-\mu_1}{\sigma_1}\right), & x < 0, \\ \frac{1}{\sigma_2} \phi\left(\frac{x-\mu_2}{\sigma_2}\right), & x > 0, \end{cases} \quad (20)$$

with associated CDF $\bar{\Phi}_s$. We refer to this distribution as a switched normal distribution, since depending on the sign of x , this distribution switches between $\mathcal{N}(\mu_1(t), \sigma_1^2)$ and $\mathcal{N}(\mu_2(t), \sigma_2^2)$. A visualization of this distribution can be found in Fig. 2 (right).

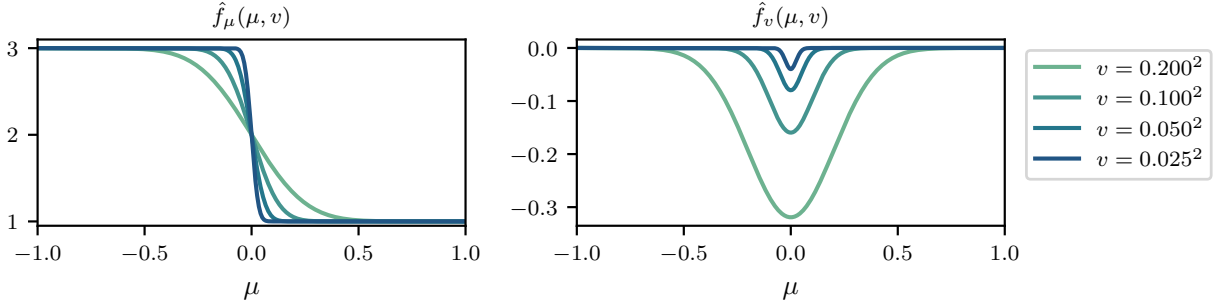


Figure 3: The approximated mean and variance dynamics (21) for the system from Example 6.

4.2. Approximate uncertainty dynamics via normalization

Even though we can derive analytical results for the specific case considered in the previous subsection, we can see that already in such a simple scenario this becomes rather involved. If we want to consider more general situations, the above results are of limited use. A large part of the complexity came from the fact that the state was not distributed normally. In the following we will see what happens if at each time we approximate the true distribution by a normal distribution. This will allow us to derive an explicit ODE for mean and variance.

Proposition 7. *Consider the IVP with state $x \in \mathbb{R}$, $x(0) = x_0$, $\dot{x} = f(x)$, $t \in \mathbb{T}$, with piecewise constant f of the form (18), and with $x_0 \sim \mathcal{N}(\mu, v)$ where $v = \sigma^2$. Then for the corresponding IVP in μ and v as defined by (14), such that $\mathcal{N}(\mu(t), v(t))$ is an approximation of the exact distribution at time t , we can state the right-hand side explicitly as*

$$\dot{\mu} = \bar{f}_1 \Phi\left(\frac{-\mu}{\sqrt{v}}\right) + \bar{f}_2 \left(1 - \Phi\left(\frac{-\mu}{\sqrt{v}}\right)\right), \quad (21a)$$

$$\dot{v} = 2(\bar{f}_2 - \bar{f}_1) \frac{1}{\sqrt{v}} \phi\left(-\frac{\mu}{\sqrt{v}}\right) v. \quad (21b)$$

Proof. For the mean dynamics we have from (6a) that

$$\dot{\mu} = \mathbb{E}_{x \in \mathcal{N}(\mu, v)}\{f(x)\} = \int_{-\infty}^0 \bar{f}_1 \frac{1}{\sqrt{v}} \phi\left(\frac{x-\mu}{\sqrt{v}}\right) dx + \int_0^\infty \bar{f}_2 \frac{1}{\sqrt{v}} \phi\left(\frac{x-\mu}{\sqrt{v}}\right) dx \quad (22a)$$

$$= \bar{f}_1 \Phi\left(\frac{-\mu}{\sqrt{v}}\right) + \bar{f}_2 \left(1 - \Phi\left(\frac{-\mu}{\sqrt{v}}\right)\right), \quad (22b)$$

where in the last step we used Lemma 5. The variance dynamics follow from Lemma 2. \square

As it turns out, the mean dynamics (21a) are exactly a form of smoothing of the form (2), with smoothing function $\alpha_\sigma(\xi) = \Phi(\frac{\xi}{\sigma})$. This is visualized in Fig. 3.

Example 8. We apply dynamics (21) to the system from Example 6 with initial distribution $x_0 \sim \mathcal{N}(\bar{\mu}_1, \sigma_1)$ and compare the resulting evolution of $\mu(t)$ and $\sigma^2(t)$ to mean and variance of the exactly propagated switched normal distribution (19). While the initial distribution is not exactly identical to a switched normal distribution, the mean is at a distance of more than 6 standard deviations from the switching surface, such that the initial probability mass on the other side of the switching surface is less than 10^{-9} , and difference between the two distributions is negligible. The resulting errors over time are shown in Fig. 4. Some error is accumulated while the distribution is crossing the switch, but the error is constant before and after.

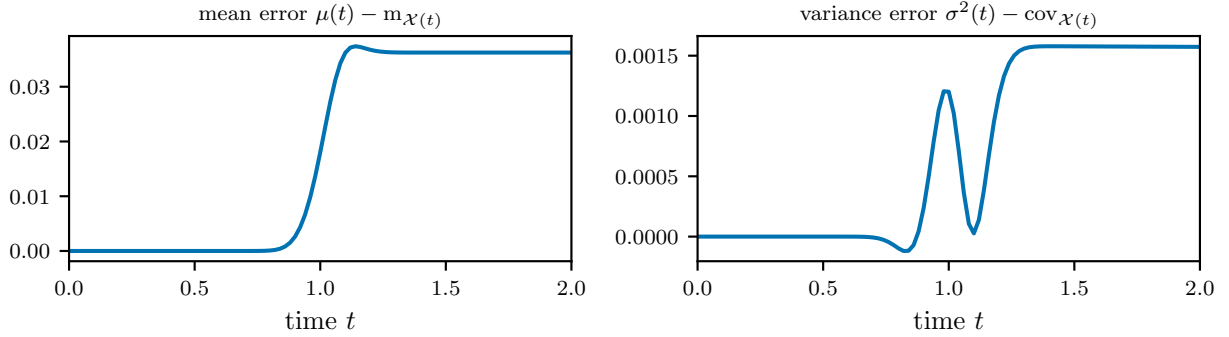


Figure 4: Left: error between exact and approximated mean over time. Right: error between exact and approximated variance over time.

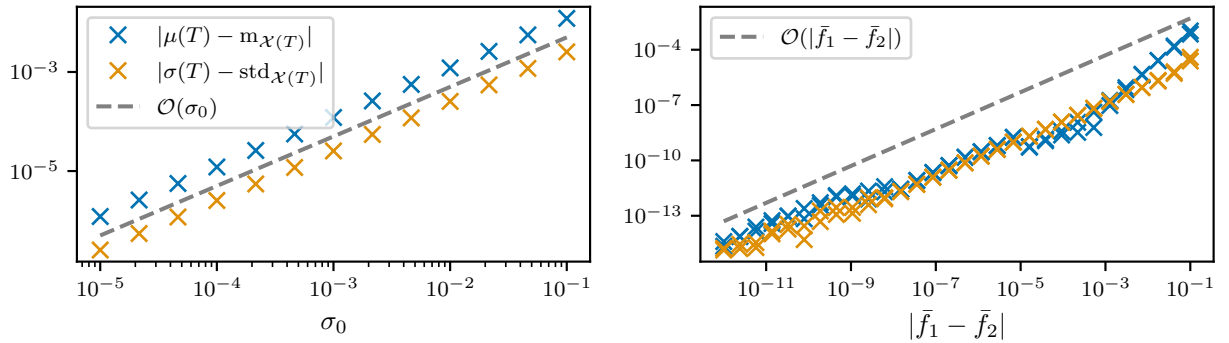


Figure 5: Left: Final integration error as a function of initial variance. Right: Final integration error as a function of the jump in dynamics. The plot includes both the case where $\bar{f}_1 - \bar{f}_2$ is positive and where it is negative.

We now perform two experiments on the influence of parameters on the total error that is accumulated during the crossing of the switch. Strictly speaking the switching process is never completed nor does it have a well defined starting point due to the unbounded support of the normal distributions. We use the error at time T as a proxy for the total error while ensuring that both initial and final mean have distance of at least six standard deviations from the switching surface in their respective direction. Thus, the probability mass which has not yet switched at the end can be neglected. In the first experiment, we vary the initial standard deviation σ_0 , with fixed $\bar{f}_1 = 3$, $\bar{f}_2 = 1$, $T = 2$. The results are shown in Fig. 5 (left). In the second experiment we vary the pre-switching dynamics \bar{f}_1 while keeping the post-switching dynamics fixed at $\bar{f}_2 = 1$, with initial standard deviation $\sigma_0 = 0.3$ and $T = 4$. For $\bar{f}_1 = \bar{f}_2$ we would expect no error since in this case there is no discontinuity, and an error that continuously rises as $|\bar{f}_1 - \bar{f}_2|$ moves away from zero. Thus, we vary \bar{f}_1 both in the interval $[\bar{f}_2 + 10^{-12}, \bar{f}_2 + 10^{-1}]$ and $[\bar{f}_2 - 10^{-12}, \bar{f}_2 - 10^{-1}]$. The results are shown in Fig. 5 (right). In combination these experiments suggest that the final integration error is of order $\mathcal{O}(\sigma_0 |\bar{f}_1 - \bar{f}_2|)$. While we do not investigate this in detail here, we point out that this is consistent with the error resulting from smoothing the discontinuity in the nominal case, cf. [12].

5. Uncertainty propagation for piecewise affine systems

After having developed an understanding of how a normal distribution behaves when passing through the discontinuity of an ODE with piecewise constant right-hand side, we now consider the more general case of a piecewise affine system with affine switching function,

$$f(x) := \begin{cases} A_1 x + \bar{f}_1, & g^\top(x - \bar{x}) < 0, \\ A_2 x + \bar{f}_2, & g^\top(x - \bar{x}) > 0. \end{cases} \quad (23)$$

In this case the switching surface is a hyper plane $\{x \in \mathbb{R}^n \mid g^\top(x - \bar{x}) = 0\}$ with normal vector $g \in \mathbb{R}^n$ and $\bar{x} \in \mathbb{R}^n$ an arbitrary point on the surface.

While in the piecewise constant case a normal distribution is asymptotically recovered after crossing a discontinuity, this is not generally true in the piecewise affine case. However, similarly to the switched constant case, during the switching process the distribution will be strongly different from a normal distribution, but after crossing the resulting distribution will resemble a slightly perturbed normal distribution.

For this case we will not try to find an exact parameterization of the distribution as it encounters the switching surface. Instead, we will directly derive approximate dynamics for mean and variance and validate them by sampling. Before stating these dynamics we define by $\tilde{\phi}_g(\xi; \mu, \Sigma)$ the PDF of the univariate normal distribution obtained by projecting the n -variate distribution $\mathcal{N}(\mu, \Sigma)$ onto the direction $g \in \mathbb{R}^n$,

$$\tilde{\phi}_g(\xi; \mu, \Sigma) := \frac{1}{\sqrt{g^\top \Sigma g}} \phi\left(\frac{\xi - g^\top \mu}{\sqrt{g^\top \Sigma g}}\right), \quad (24)$$

where $\xi \in \mathbb{R}$ is the remaining degree of freedom after projection, and which has mean $\mu_g := g^\top \mu$, standard deviation $\sigma_g := \sqrt{g^\top \Sigma g}$ and associated CDF $\tilde{\Phi}_g(\xi; \mu, \Sigma)$. Similarly, the projection of \bar{x} is denoted by $\bar{x}_g := g^\top \bar{x}$

Proposition 9. *Consider an IVP with state $x \in \mathbb{R}^n$, $x(0) = x_0$, $\dot{x} = f(x)$, $t \in \mathbb{T}$, $x_0 \sim \mathcal{N}(\mu, \Sigma)$, and with $f(x)$ piecewise affine with affine switching function as in (23). Then for the corresponding IVP in μ and Σ as defined by (14), such that $\mathcal{N}(\mu(t), \Sigma(t))$ is an approximation of the exact distribution at time t , we can state the right-hand side explicitly as*

$$\dot{\mu} = \hat{f}_\mu(\mu, \Sigma), \quad \dot{\Sigma} = \underbrace{\frac{\partial \hat{f}_\mu(\mu, \Sigma)}{\partial \mu} \Sigma + \Sigma \frac{\partial \hat{f}_\mu(\mu, \Sigma)}{\partial \mu}}_{=: \hat{f}_\Sigma(\mu, \Sigma)}^\top \quad (25)$$

with

$$\hat{f}_\mu(\mu, \Sigma) := (A_2 - A_1) \Sigma g \tilde{\phi}_g(\bar{x}_g; \mu, \Sigma) + f_1(\mu) \tilde{\Phi}_g(\bar{x}_g; \mu, \Sigma) + f_2(\mu) (1 - \tilde{\Phi}_g(\bar{x}_g; \mu, \Sigma)), \quad (26a)$$

$$\begin{aligned} \hat{f}_\Sigma(\mu, \Sigma) := & (A_2 - A_1) \frac{\Sigma g g^\top \Sigma}{g^\top \Sigma g} (\bar{x}_g - g^\top \mu) \tilde{\phi}_g(\bar{x}_g; \mu, \Sigma) + (f_2(\mu) - f_1(\mu)) g^\top \Sigma \tilde{\phi}_g(\bar{x}_g; \mu, \Sigma) \\ & + A_1 \Sigma \tilde{\Phi}_g(\bar{x}_g; \mu, \Sigma) + A_2 \Sigma (1 - \tilde{\Phi}_g(\bar{x}_g; \mu, \Sigma)) + (\star). \end{aligned} \quad (26b)$$

Corollary 10. *Consider the same situation as in Prop. 9 and additionally assume $A_1 = A_2 =: A$. Then*

$$\hat{f}_\mu(\mu, \Sigma) = A\mu + \bar{f}_1 \tilde{\Phi}_g(\bar{x}_g; \mu, \Sigma) + \bar{f}_2 (1 - \tilde{\Phi}_g(\bar{x}_g; \mu, \Sigma)), \quad (27)$$

$$\hat{f}_\Sigma(\mu, \Sigma) = (\bar{f}_2 - \bar{f}_1) g^\top \Sigma \tilde{\phi}_g(\bar{x}_g; \mu, \Sigma) + A\Sigma + (\star). \quad (28)$$

Proof. Without loss of generality we state the proof under the assumption that the switching function gradient is given by $g = (1, 0, \dots, 0)$, such that the first dimension of the state space is orthogonal to the switching surface. If this assumption does not hold one may substitute $y = Rx$, with invertible $R \in \mathbb{R}^{n \times n}$, such that in the transformed state space the assumption holds. We use Lemma 2 to derive (26). The basic structure of the proof is to separate the expectation in (12a) into two steps: the expectation over the first dimension, in which the switch occurs, and the conditional expectation over the remaining dimensions, with respect to which the dynamics are linear. We partition the state space as

$$x \sim \mathcal{N}(\mu, \Sigma), \quad x = \begin{bmatrix} x_1 \\ x_2 \end{bmatrix}, \quad \mu = \begin{bmatrix} \mu_1 \\ \mu_2 \end{bmatrix}, \quad \Sigma = \begin{bmatrix} \sigma_g^2 & \Sigma_{12} \\ \Sigma_{21} & \Sigma_{22} \end{bmatrix}, \quad (29)$$

where $x_1, \mu_1 \in \mathbb{R}$, $x_2, \mu_2 \in \mathbb{R}^{n-1}$, $\sigma_g^2 \in \mathbb{R}$, $\Sigma_{22} \in \mathbb{S}^{n-1}$ and Σ_{21}, Σ_{12} correspondingly. We use $\sigma_g^2 = g^\top \Sigma g$ instead of Σ_{11} to emphasize that in x_1 we have a univariate distribution resulting from projecting $\mathcal{N}(\mu, \Sigma)$ onto the direction g .

From (12a) we get the mean dynamics as

$$\hat{f}_\mu(\mu, \Sigma) = \mathbb{E}_{x \sim \mathcal{N}(\mu, \Sigma)}\{f(x)\} = \mathbb{E}_{x_1}\{\mathbb{E}_{x_2|x_1}\{f(x)\}\} \quad (30a)$$

$$= \mathbb{E}_{x_1}\{f(\mathbb{E}_{x_2|x_1}\{x\})\} = \mathbb{E}_{x_1 \sim \mathcal{N}(\mu_1, \sigma_g^2)}\{f(\check{\mu}(x_1)\} \quad (30b)$$

where we first use conditional expectation and then move the expectation over x_2 into $f(\cdot)$ which is allowed since the switch depends only on x_1 such that $f(\cdot)$ is affine in x_2 . For the inner expectation we use $\mathbb{E}_{x_2|x_1}\{x_1\} = x_1$ and $\mathbb{E}_{x_2|x_1}\{x_2\} = \mu_2 + \Sigma_{21}\sigma_g^{-2}(x_1 - \mu_1)$ due to $x \sim \mathcal{N}(\mu, \Sigma)$ such that over all

$$\check{\mu}(x_1) := \mathbb{E}_{x_2|x_1}\{x\} = \begin{bmatrix} 1 \\ \Sigma_{21}\sigma_g^{-2} \end{bmatrix} x_1 + \begin{bmatrix} 0 \\ \mu_2 - \Sigma_{21}\sigma_g^{-2}\mu_1 \end{bmatrix}. \quad (31)$$

Defining

$$a_i := A_i \begin{bmatrix} 1 \\ \Sigma_{21}\sigma_g^{-2} \end{bmatrix}, \quad b_i := A_i \begin{bmatrix} 0 \\ \mu_2 - \Sigma_{21}\sigma_g^{-2}\mu_1 \end{bmatrix} + \bar{f}_1, \quad i = 1, 2. \quad (32)$$

allows us to write

$$f(\check{\mu}(x_1)) = \begin{cases} a_1 x_1 + b_1, & x_1 - \bar{x}_1 < 0, \\ a_2 x_1 + b_2, & x_1 - \bar{x}_1 > 0, \end{cases} \quad (33)$$

where $\bar{x}_1 \in \mathbb{R}$ results from the partitioning of $\bar{x} = (\bar{x}_1, \bar{x}_2)$. Continuing (30), we get

$$\hat{f}_\mu(\mu, \Sigma) = \mathbb{E}_{x_1 \sim \mathcal{N}(\mu_1, \sigma_g^2)}\{f(\check{\mu}(x_1))\} \quad (34a)$$

$$= \int_{-\infty}^{\bar{x}_1} (a_1 x_1 + b_1) \frac{1}{\sigma_g} \phi\left(\frac{x_1 - \mu_1}{\sigma_g}\right) dx_1 + \int_{\bar{x}_1}^{\infty} (a_2 x_1 + b_2) \frac{1}{\sigma_g} \phi\left(\frac{x_1 - \mu_1}{\sigma_g}\right) dx_1 \quad (34b)$$

$$= (a_2 - a_1) \sigma_g^2 \frac{1}{\sigma_g} \phi\left(\frac{\bar{x}_1 - \mu_1}{\sigma_g}\right) + (a_1 \mu_1 + b_1) \Phi\left(\frac{\bar{x}_1 - \mu_1}{\sigma_g}\right) + (a_2 \mu_1 + b_2) (1 - \Phi\left(\frac{\bar{x}_1 - \mu_1}{\sigma_g}\right)), \quad (34c)$$

where the last line results from applying Lemma 5 to each row of the integrated function. Resubstitution of a_i, b_i yields

$$a_i \mu_1 + b_i = A_i \mu + \bar{f}_i = f_i(\mu), \quad a_i \sigma_g^2 = A_i \Sigma g, \quad i = 1, 2, \quad (35)$$

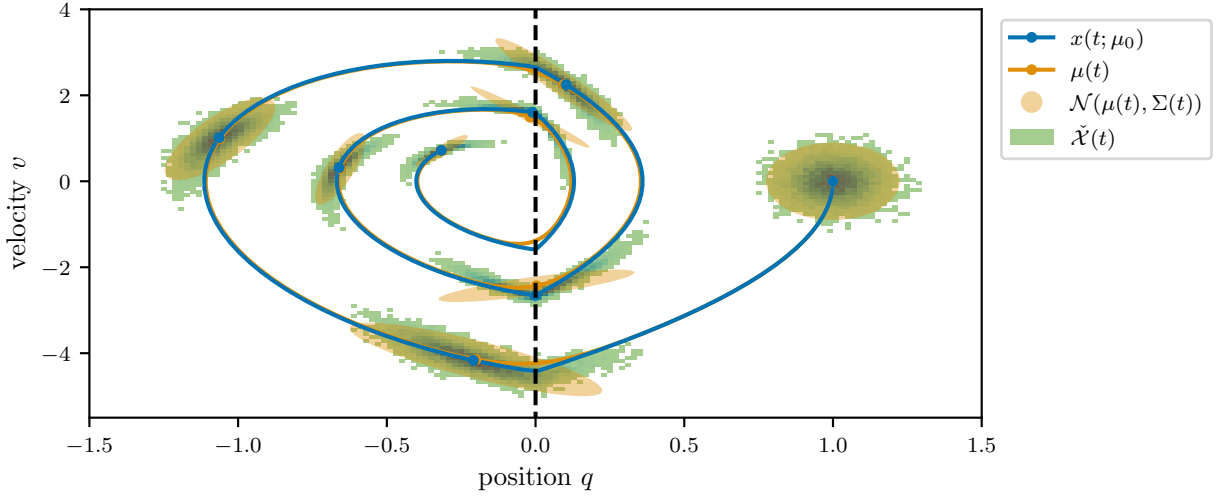


Figure 6: Trajectories for the switched system from Example 11 in state space with histograms of the sampling distribution $\tilde{\mathcal{X}}$ in comparison with the approximating normal distribution shown for selected times.

such that

$$\hat{f}_\mu(\mu, \Sigma) = (A_2 - A_1)\Sigma g \tilde{\phi}_g(\bar{x}; \mu, \Sigma) + f_1(\mu)\tilde{\Phi}_g(\bar{x}; \mu, \Sigma) + f_2(\mu)(1 - \tilde{\Phi}_g(\bar{x}; \mu, \Sigma)), \quad (36)$$

which is identical to (26a). The variance dynamics (26b) follow from Lemma 2. \square

As already discussed in the previous section this approximation is heuristic in that it does not allow for an arbitrarily small error for any given system in the form (23), since the error cannot be influenced by choice of hyper parameters. However, the approximation is principled in the following sense: (a) If $A_1 = A_2$ and $\tilde{f}_1 = \tilde{f}_2$, i.e., if effectively there is no discontinuity, the corresponding Lyapunov equation for a linear system is recovered [18]. (b) With increasing distance of the mean from the switching surface, as measured in terms of the projected standard deviation σ_g , both $\tilde{\phi}_g(\bar{x}_g; \mu, \Sigma)$ and $\tilde{\Phi}_g(\bar{x}_g; \mu, \Sigma)$ decay exponentially to 0 resp. 1. Thus, the Lyapunov dynamics for the corresponding mode are recovered asymptotically.

Example 11. We consider a linear spring/dashpot contact-impact model [3]. The system has state $x = (q, v)$ with position $q \in \mathbb{R}$ and velocity $v \in \mathbb{R}$. The position $q = 0$ corresponds to the system being in contact with a wall but with uncompressed spring. For $q < 0$ the system is in contact and the spring is compressed such that $\dot{v} = -kq - cv$, with spring constant k and damping c . For $q > 0$ there is no contact and the spring is uncompressed. However, an external force of magnitude g is applied, pushing the mass towards the wall. Thus in this case $\dot{v} = -g$. Overall, the dynamics can be written as

$$\dot{x} = \begin{cases} f_1(x), & \psi(x) < 0, \\ f_2(x), & \psi(x) > 0, \end{cases} \quad f_1(x) = \begin{bmatrix} x_2 \\ -g \end{bmatrix}, \quad f_2(x) = \begin{bmatrix} x_2 \\ -kx_1 - cx_2 \end{bmatrix}, \quad \psi(x) = -x_1. \quad (37)$$

The initial state is distributed as $x_0 \sim \mathcal{X}_0 = \mathcal{N}(\mu_0, \Sigma_0)$. We simulate the system based on the approximate dynamics (25) for mean and covariance yielding a time varying normal distribution $\mathcal{N}(\mu(t), \Sigma(t))$. As proxy for the exact evolution of the distribution we sample 10^4 points from \mathcal{X}_0

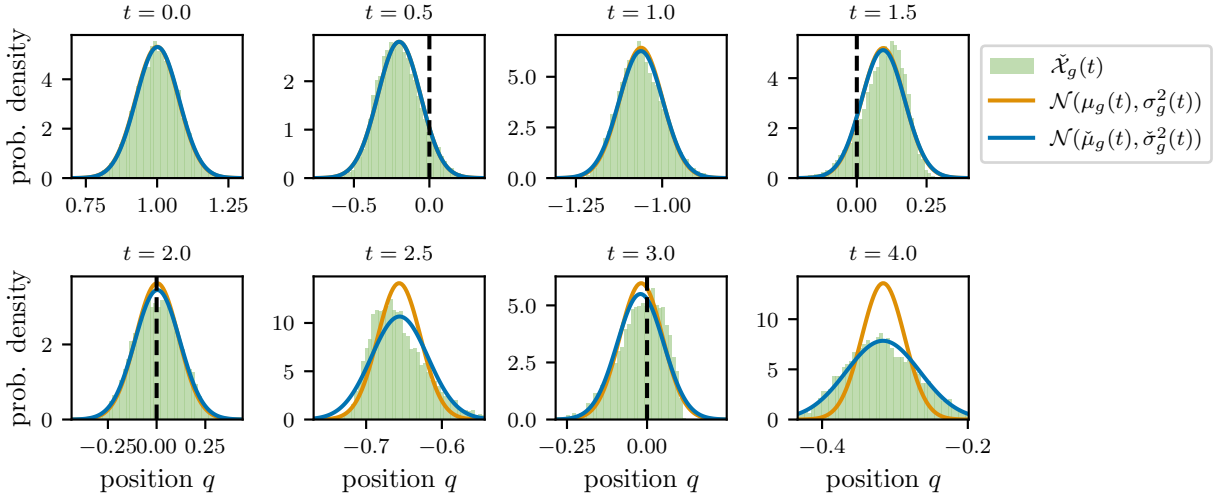


Figure 7: The state distributions for the switched system from Example 11 at selected times projected onto the (negative) switching surface gradient direction. Compared are the sample distribution $\check{\mathcal{X}}(t)$, the normal distribution $\mathcal{N}(\check{\mu}_g(t), \check{\sigma}_g^2(t))$ that has the same mean and variance as the sample distribution, and the normal distribution $\mathcal{N}(\mu_g(t), \sigma_g^2(t))$ resulting from the approximate propagation of mean and variance through (26).

and propagate them based on the nonsmooth dynamics, yielding the sample distribution $\check{\mathcal{X}}(t)$ with $\check{\mathcal{X}}(0) \approx \mathcal{X}_0$ and associated mean $\check{\mu}_g(t) = m_{\check{\mathcal{X}}(t)}$ and covariance $\check{\Sigma}(t) = \text{cov}_{\check{\mathcal{X}}(t)}$. We also consider the propagation of the original mean μ_0 through the nonsmooth dynamics, denoted by $x(t; \mu_0)$, since for this example it will always correspond to the mode of the exactly propagated distribution. The results are shown in Fig. 6. For the sample distribution it can be seen that it becomes strongly deformed – like a kink – when crossing a switch but mostly recovers when each samples has passed, cf. Fig. 6 and 7. However some small deformation with respect to a normal distribution remains and accumulates with each switch. When looking at the distribution projected onto the switching surface gradient g , Fig. 7, the non-normalcy seems a lot less severe. This is relevant since only this projected distribution is used in the dynamics (26).

6. Uncertainty propagation for piecewise smooth systems

We return to the general case of (1) where the right-hand side of the ODE takes the form

$$f(x) = \begin{cases} f_1(x), & \psi(x) < 0, \\ f_2(x), & \psi(x) > 0, \end{cases} \quad (38)$$

with smooth nonlinear components f_1, f_2, ψ . Given the results for the piecewise affine case from the previous section, we show how they can be applied in this more general setting, based on linearization. In contrast to the standard linearization based approaches, cf. (8) and (10), which would linearize the full integration map resp. the smooth approximation (2) of the right-hand side, we linearize only the components of (38) such that the specific structure of the discontinuity is preserved. We call

$$f_{\text{lin,pw}}(x; \mu) = \begin{cases} f_1(\mu) + \nabla f_1(\mu)^\top (x - \mu), & \psi(\mu) + \nabla \psi(\mu)^\top (x - \mu) < 0, \\ f_2(\mu) + \nabla f_2(\mu)^\top (x - \mu), & \psi(\mu) + \nabla \psi(\mu)^\top (x - \mu) > 0, \end{cases} \quad (39)$$

the piecewise linearization of f at μ , which is identical to f if f is piecewise affine. After this piecewise linearization, the results of Proposition 9 can in principle be applied, but with some additional dependencies on μ . The resulting dynamics are

$$\dot{\mu} = \hat{f}_\mu(\mu, \Sigma), \quad \dot{\Sigma} = \hat{f}_\Sigma(\mu, \Sigma), \quad (40)$$

with

$$\hat{f}_\mu(\mu, \Sigma) := (\nabla f_2(\mu) - \nabla f_1(\mu))^\top \Sigma \nabla \psi(\mu) \frac{1}{\sigma_\psi(\mu, \Sigma)} \phi\left(\frac{-\psi(\mu)}{\sigma_\psi(\mu, \Sigma)}\right) \quad (41a)$$

$$+ (f_1(\mu) + \nabla f_1(\mu)^\top (x - \mu)) \Phi\left(\frac{-\psi(\mu)}{\sigma_\psi(\mu, \Sigma)}\right) \quad (41b)$$

$$+ (f_2(\mu) + \nabla f_2(\mu)^\top (x - \mu)) \left(1 - \Phi\left(\frac{-\psi(\mu)}{\sigma_\psi(\mu, \Sigma)}\right)\right), \quad (41c)$$

$$\hat{f}_\Sigma(\mu, \Sigma) := \frac{\partial \hat{f}_\mu(\mu, \Sigma)}{\partial \mu} \Sigma + \Sigma \frac{\partial \hat{f}_\mu(\mu, \Sigma)}{\partial \mu}^\top, \quad (41d)$$

where $\sigma_\psi(\mu, \Sigma) := \sqrt{\nabla \psi(\mu)^\top \Sigma \nabla \psi(\mu)}$ is the standard deviation orthogonal to the switching surface with respect to the linearization of ψ at μ . Due to the additional dependencies of $\hat{f}_\mu(\mu, \Sigma)$ on μ the explicit expression for $\hat{f}_\Sigma(\mu, \Sigma)$ is more involved than (26b). However, if these equations are implemented with a symbolic framework such as CasADi [23] there is no need to derive the explicit expressions by hand. In the case that f_1 , f_2 , and ψ are affine, the expressions in (41) simplify to those of (26).

7. Stochastic optimal control problem formulation

We now demonstrate how the derived dynamics can be used within a stochastic OCP formulation. After augmenting the dynamics by an argument for the control vector $u(t) \in \mathbb{R}^{n_u}$ – which for the purpose of integration can be seen as a time dependent parameter – a rather general OCP can be stated as

$$\min_{u(\cdot), \mu(\cdot), \Sigma(\cdot)} \int_0^T l(\mu(t), u(t)) dt + L(\mu(T)) \quad (42a)$$

$$\text{s.t.} \quad \mu(0) = \bar{\mu}_0, \quad \Sigma(0) = \bar{\Sigma}_0, \quad (42b)$$

$$\dot{\mu}(t) = \hat{f}_\mu(\mu(t), \Sigma(t), u(t)), \quad t \in [0, T], \quad (42c)$$

$$\dot{\Sigma}(t) = \hat{f}_\Sigma(\mu(t), \Sigma(t), u(t)), \quad t \in [0, T], \quad (42d)$$

$$0 \geq g(u(t)), \quad t \in [0, T], \quad (42e)$$

$$0 \geq h^i(\mu(t)) + \gamma \sqrt{\nabla h^i(\mu(t))^\top \Sigma(t) \nabla h^i(\mu(t))}, \quad t \in [0, T], \quad i = 1, \dots, n_h. \quad (42f)$$

Here we consider stage cost l and terminal cost L only for state mean μ and controls u , but it could be straightforwardly extended by a direct cost on the variance Σ . The initial mean and covariance are fixed to $\bar{\mu}_0$ resp. $\bar{\Sigma}_0$. For simplicity of notation we consider separate constraints on controls, $g(u) \leq 0$, $g: \mathbb{R}^{n_x} \rightarrow \mathbb{R}^{n_g}$, and states, $h(x) \leq 0$, $h: \mathbb{R}^{n_u} \rightarrow \mathbb{R}^{n_h}$, although the formulation can be straightforwardly generalized to combined constraints. Since $x \in \mathcal{N}(\mu, \Sigma)$ has unbounded support the state constraints cannot be strictly enforced for all possible values of x . Instead we

use individual chance constraints in each component $h^i(x)$, $i = 1, \dots, n_h$, requiring that at each time t (individually) the probability of constraint satisfaction should be at least p ,

$$\text{Prob}_{x \sim \mathcal{N}(\mu, \Sigma)} \{h^i(x) \leq 0\} \geq p. \quad (43)$$

After linearization of $h(x)$ at μ and for $\frac{1}{2} < p < 1$, a tractable approximation can be written as

$$h^i(\mu) + \gamma(p) \sqrt{\nabla h^i(\mu)^\top \Sigma \nabla h^i(\mu)} \leq 0, \quad (44)$$

which consists of the constraint function evaluated at the mean plus an additional backoff term. The backoff term is given by the standard deviation in direction orthogonal to the linearized constraint scaled by $\gamma(p) = \Phi^{-1}(p)$, with $\Phi^{-1}(p)$ the inverse CDF of the standard normal distribution.

The resulting OCP (42) can then be treated by standard methods of direct optimal control [5] to obtain a nonlinear program (NLP) which can be solved via numerical optimization [6].

For the examples considered in the following we discretize the time interval $[0, T]$ into an equidistant grid of N intervals, such that the corresponding step length is $h = T/N$, and enumerate the grid points by $k = 0, \dots, N$. Within each interval a constant control $u_k \in \mathbb{R}^{n_u}$ is applied. Integration of the approximate mean and covariance dynamics (26) over each time interval results in the discretized dynamics

$$(\mu_{k+1}, \Sigma_{k+1}) = F(\mu_k, \Sigma_k, u_k), \quad k = 0, \dots, N-1, \quad (45)$$

which here we obtain by applying one step of the explicit Runge-Kutta method of fourth order (RK4). Choosing a multiple shooting formulation [24] the resulting discretized OCP is an NLP of the form

$$\min_{\substack{u_0, \dots, u_{N-1}, \\ \mu_0, \dots, \mu_N, \\ \Sigma_0, \dots, \Sigma_N}} \sum_{k=0}^{N-1} h l(\mu_k, u_k) + L(\mu_N) \quad (46a)$$

$$\text{s.t.} \quad \mu_0 = \bar{\mu}_0, \quad \Sigma_0 = \bar{\Sigma}_0, \quad (46b)$$

$$0 = F(\mu_k, \Sigma_k, u_k) - (\mu_{k+1}, \Sigma_{k+1}), \quad k = 0, \dots, N-1, \quad (46c)$$

$$0 \geq g(u_k), \quad k = 0, \dots, N-1, \quad (46d)$$

$$0 \geq h^i(\mu_k) + \gamma \sqrt{\nabla h^i(\mu_k) \Sigma_k \nabla h^i(\mu_k)^\top}, \quad i = 1, \dots, n_h, \quad k = 1, \dots, N. \quad (46e)$$

While the covariances Σ_k are guaranteed to be positive definite at a solution if $\bar{\Sigma}_0 \succ 0$, they may take arbitrarily indefinite values throughout the solver iterations which can cause problems due to the square root in (46e). To avoid this one may use decoupling slack variables, cf. [25, 26]. In the following examples we formulate the respective OCP of form (46) via the Python interface of the symbolic framework CasADI [23] and solve them with the interior point method IPOPT [27].

Example 12 (Quadcopter with wind shadow). We consider a quadcopter described by state $x = (p_x, p_y, v_x, v_y) \in \mathbb{R}^4$, i.e., position and velocity in both x and y direction. The control vector $u = (u_x, u_y)$ consists of acceleration in the two directions.

We consider two air layers with different wind speeds: If $p_y < 0$ there is no wind due to obstacles blocking its path, and for $p_y > 0$ there is wind in p_x -direction with $v_w = -1$. In both layers we consider air friction in p_x -direction with drag coefficient $d = 0.01$. The dynamics are thus

$$\dot{p}_x = v_x, \quad \dot{p}_y = v_y, \quad \dot{v}_y = u_y, \quad \dot{v}_x = \begin{cases} u_x - d|v_x|v_x, & p_y < 0, \\ u_x - d|v_x - v_w|(v_x - v_w), & p_y > 0. \end{cases} \quad (47)$$

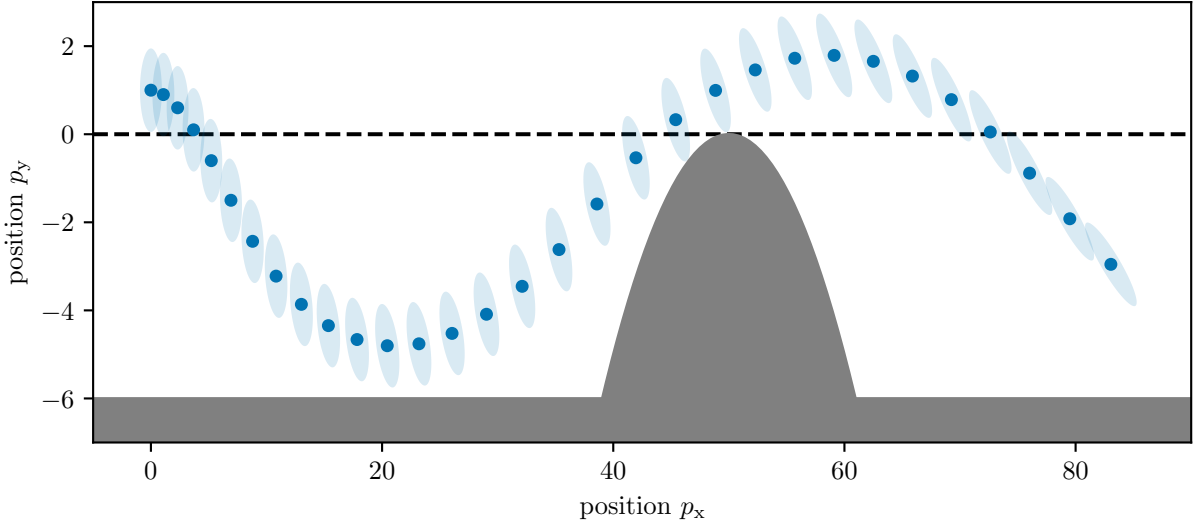


Figure 8: Optimal trajectory for the quadcopter from example 12. Shown are the mean and the 99% confidence region of the normal distribution. The dashed line indicates the switching surface, the infeasible region is darkly shaded.

For the considered trajectories we will always have $v_x > 0$ such that the non-differentiability of the absolute value will not become relevant. Starting from a fixed initial position the control aim is to maximize the p_x position in the given time window, $l(x, u) = -p_x + \epsilon \|u\|_2^2$, $L(x) = -p_x$, where the controls are slightly regularized with $\epsilon = 10^{-5}$. The car should stay above the lower bound of $p_y \geq p_{y,\min}$ with $p_{y,\min} = 6$ and in one region the path is blocked by a parabolic obstacle modelled as $p_y \geq 0.05(p_x - 40)^2$. The controls are constrained as $\|u\|_\infty \leq 5$. The initial state is uncertain with $x_0 \sim \mathcal{N}(\bar{\mu}_0, \bar{\Sigma}_0)$ where $\bar{\mu}_0 = (0, 1, 5, 0)$ and $\bar{\Sigma}_0 = \text{diag}(10^{-1}, 10^{-1}, 10^{-5}, 10^{-5})$. We discretize the time interval into $N = 30$ intervals of length $h = 0.2$ and solve the corresponding OCP of form (46). The solution is visualized in Fig. 8. The quadcopter starts by moving downwards to get into the wind shadow of the obstacle. Due to the obstacle it has to leave the wind shadow after some time, but does so only as long as necessary. Since the quadcopter is slowed down more in the upper region this has a rotating effect on the covariance whenever the distribution has nonnegligible support in both lanes.

Example 13 (Implicit constraint). We consider a two-dimensional system with state $x = (p_x, p_y) \in \mathbb{R}^2$. The controls are $u = (u_x, u_y)$, constrained by $\|u\|_\infty \leq u_{\max}$ with $u_{\max} = 2$. In one region of the state space these are directly the velocities of the system, but in the other region there is an additional vector field, which is in magnitude stronger than the control constraints. More specifically we have $f_1(x, u) = u - (4.5, 5)u_{\max}$, $f_2(x, u) = u$ and $\psi(x) = -p_y - p_x^2$. The control goal is to steer the system to the target position $x_{\text{goal}} = (6, -2)$ for which we use Huber-like cost terms $l(x, u) = \|(x, \varepsilon_H)\|_2 + \varepsilon_u \|u\|_2^2$, $L(x) = \|(x, \varepsilon_H)\|_2$, with Huber smoothing $\varepsilon_H = \sqrt{0.5}$ and slight control regularization $\varepsilon_u = 10^{-5}$. The initial value is distributed as $x_0 \sim \mathcal{N}(\bar{\mu}_0, \bar{\Sigma}_0)$ where $\bar{\mu}_0 = (-6.5, -2)$ and $\bar{\Sigma}_0 = \frac{1}{4} \text{diag}(1, 1)$. We discretize the time interval into $N = 15$ intervals of length $h = 0.5$ and solve the corresponding OCP of form (46).

The solution is visualized in Fig. 9 (left), where we additionally sample 50 values from the initial

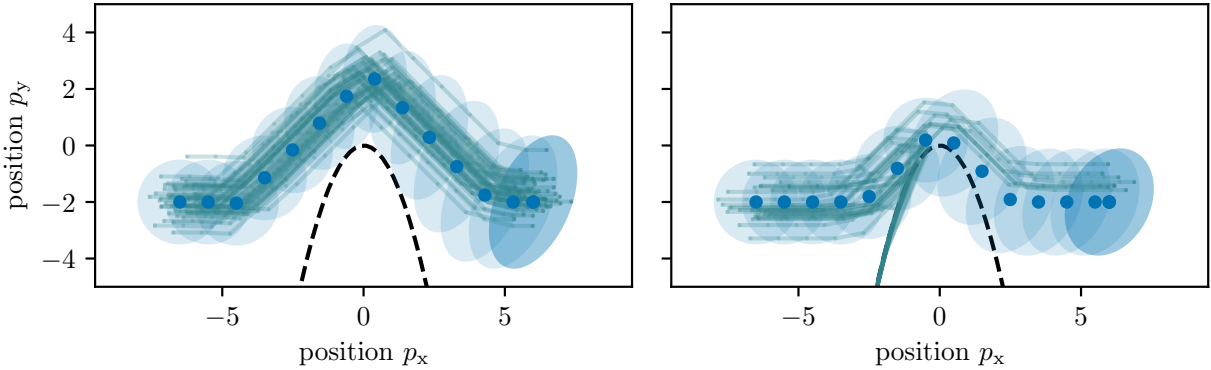


Figure 9: Optimal solutions when using either the approximate dynamics (25) (left) or the standard linearization based approach (10)(right), indicated by blue dots for the mean and a shaded 99% confidence region. The green lines are samples from the initial distribution simulated according to the respective optimal control trajectory (open loop).

distribution and simulate their trajectories with NOSNOC [28] based on the optimal control trajectory (open loop). Since in the region with f_1 the additional vector field is too strong given the control constraints, $\psi(x)$ acts like an implicit constraint, and the region is mostly avoided.

We compare this to the standard linearization based approach (10) applied to the smoothed dynamics (2) with smoothing parameter $\sigma = 5 \cdot 10^{-2}$. Since in these the covariance propagation is based on linearization at the mean, the resulting dynamics only “see” the switch if the mean is in its vicinity, independent of the level of uncertainty. Thus, in the resulting optimal trajectory, cf. Fig 9 (right), the mean keeps almost no distance from the switching surface, with a significant amount of probability mass overlapping with the second region. In consequence, when simulating the sample distribution, a large fraction of the samples gets trapped in this region and does not arrive at the target state.

8. Conclusions

We derived a method for the approximate propagation of mean and variance through an ODE with discontinuous right-hand side and demonstrated how it can be straightforwardly used in a stochastic OCP formulation. However, the paper was mostly focused on the derivation of the approximations. A formal analysis of the resulting errors would enable a more rigorous theoretical backing of the method. Further, we only treated the case of two different modes of the right-hand side. If similar results were derived for the case where the right-hand side has an arbitrary number of modes, the method could be applied in a wider range of situations.

References

- [1] A. Filippov, Differential Equations with Discontinuous Righthand Sides: Control Systems, Vol. 18, Springer Science & Business Media, 1988.
- [2] V. Acary, B. Brogliato, Numerical methods for nonsmooth dynamical systems: applications in mechanics and electronics, Springer Science & Business Media, 2008.
- [3] B. Brogliato, Nonsmooth Mechanics: Models, Dynamics and Control, Springer, 2016.
- [4] A. Iserles, A First Course in the Numerical Analysis of Differential Equations, 2nd Edition, Cambridge University Press, 2008.

[5] J. B. Rawlings, D. Q. Mayne, M. M. Diehl, *Model Predictive Control: Theory, Computation, and Design*, 2nd Edition, Nob Hill, 2017.

[6] J. Nocedal, S. J. Wright, *Numerical Optimization*, 2nd Edition, Springer Series in Operations Research and Financial Engineering, Springer, 2006.

[7] B. Kouvaritakis, M. Cannon, *Model Predictive Control. Classical, Robust and Stochastic*, Springer, 2016.

[8] A. Mesbah, Stochastic model predictive control: An overview and perspectives for future research, *IEEE Control Systems Magazine* 36 (6) (2016) 30–44.

[9] S. V. Raković, *Robust Model Predictive Control*, Springer London, London, 2019, pp. 1–11. doi:10.1007/978-1-4471-5102-9_2-3.

[10] X. Feng, S. D. Cairano, R. Quirynen, Inexact Adjoint-based SQP Algorithm for Real-Time Stochastic nonlinear MPC, in: *Proceedings of the IFAC World Congress*, 2020.

[11] A. Zanelli, J. Frey, F. Messerer, M. Diehl, Zero-order robust nonlinear model predictive control with ellipsoidal uncertainty sets, *Proceedings of the IFAC Conference on Nonlinear Model Predictive Control (NMPC)* (2021). doi:<https://doi.org/10.1016/j.ifacol.2021.08.523>.

[12] D. E. Stewart, M. Anitescu, Optimal control of systems with discontinuous differential equations, *Numerische Mathematik* 114 (4) (2010) 653–695.

[13] A. Nurkanović, S. Albrecht, M. Diehl, Limits of MPCC Formulations in Direct Optimal Control with Nonsmooth Differential Equations, in: *2020 European Control Conference (ECC)*, 2020, pp. 2015–2020. doi:10.23919/ECC51009.2020.9143593.

[14] D. Stewart, A high accuracy method for solving odes with discontinuous right-hand side, *Numerische Mathematik* 58 (1) (1990) 299–328.

[15] A. Nurkanović, M. Sperl, S. Albrecht, M. Diehl, Finite Elements with Switch Detection for Direct Optimal Control of Nonsmooth Systems (2022). doi:10.48550/ARXIV.2205.05337. URL <https://arxiv.org/abs/2205.05337>

[16] P. Billingsley, *Probability and Measure*, John Wiley & Sons, 1995.

[17] R. F. Stengel, *Optimal Control and Estimation*, Dover, 1986.

[18] T. Söderström, *Discrete-time stochastic systems*, 2nd Edition, Springer, 2002.

[19] J. Gillis, M. Diehl, A positive definiteness preserving discretization method for nonlinear Lyapunov differential equations, in: *Proceedings of the IEEE Conference on Decision and Control (CDC)*, 2013.

[20] C. Kirches, A Numerical Method for Nonlinear Robust Optimal Control with Implicit Discontinuities and an Application to Powertrain Oscillations, Diploma thesis, University of Heidelberg (October 2006).

[21] J. Quiñonero-Candela, A. Girard, J. Larsen, C. E. Rasmussen, Propagation of uncertainty in bayesian kernel models – application to multiple-step ahead forecasting, *IEEE International Conference on Acoustics, Speech and Signal Processing* (2003) 701–704.

[22] S. Julier, J. Uhlmann, Unscented filtering and nonlinear estimation, *Proceedings of the IEEE* 92 (3) (2004) 401–422.

[23] J. A. E. Andersson, J. Gillis, G. Horn, J. B. Rawlings, M. Diehl, CasADI – a software framework for nonlinear optimization and optimal control, *Mathematical Programming Computation* 11 (1) (2019) 1–36. doi:10.1007/s12532-018-0139-4.

[24] H. G. Bock, K. J. Plitt, A multiple shooting algorithm for direct solution of optimal control problems, in: *Proceedings of the IFAC World Congress*, Pergamon Press, 1984, pp. 242–247.

[25] F. Messerer, M. Diehl, An efficient algorithm for tube-based robust nonlinear optimal control with optimal linear feedback, in: *Proceedings of the IEEE Conference on Decision and Control (CDC)*, 2021.

[26] F. Messerer, K. Baumgärtner, M. Diehl, A dual-control effect preserving formulation for nonlinear output-feedback stochastic model predictive control with constraints, *IEEE Control Systems Letters* 7 (1171–1176) (2023).

[27] A. Wächter, L. T. Biegler, On the implementation of an interior-point filter line-search algorithm for large-scale nonlinear programming, *Mathematical Programming* 106 (1) (2006) 25–57.

[28] A. Nurkanović, M. Diehl, NOSNOC: A software package for numerical optimal control of nonsmooth systems, *IEEE Control Systems Letters* (2022).